# ON THE EFFECT OF PROEUTECTOIDE FERRITE UPON THE FRACTURE TOUGHNESS OF WELD METAL

K. Eriksson

Dept. of Strength of Materials and Solid Mechanics,
The Royal Institute of Technology, S-100 44 Stockholm,
Sweden

## ABSTRACT

To gain insight into the relationship between fracture toughness and microstructure of weld metals produced by submerged arc welding, two weld metals representing the best and poorest fracture toughnesses within a group of ten were chosen for a metallographic and fractographic study. The characteristical differences between the weld metals are grain size of acicular ferrite and content and distribution of proeutectoide ferrite. Local brittle cleavage facettes are found to appear almost exclusively within the domains of proeutectoide ferrite. Assuming that such local fractures are decisive for the onset of unstable crack growth the difference in fracture toughness of the weld metals can be accounted for by using the Griffith crack model.

## KEY WORDS

Fracture toughness; weld metal; microstructure; proeutectoide ferrite.

## INTRODUCTION

Understanding of the relationship between microstructure and mechanical properties has always proven successful for explaining the behaviour of materials. For base metals the amount of knowledge of the relationship between microstructure and fracture behaviour is today considerable. For weld metals, however, this field is much less explored, probably due to the complexity of such materials. The experience hitherto gained indicates clearly that such studies are meaningful and contribute to the understanding of behaviour of materials.

In a previous work (Eriksson, 1979) was determined the fracture toughness of ten different weld metals produced by submerged arc welding and which are common in practice. The fracture toughness of the weld metals was found to vary greatly, from values comparable with the fracture toughness of the parent metal to approximately one third of this, a result which is in accordance with experience from practice.

To gain insight into the relationship between fracture toughness and microstructure of the weld metals, the two weld metals representing the best and poorest fracture toughnesses, respectively, within the above group were chosen for the present work comprising a fracture toughness, a metallographic and a fractographic study. The

microstructure of the weld metals and their fracture behaviour are described and the relationship with fracture toughness discussed.

## MATERIAL

The parent metal was a normalized fine grain C-Mn-steel (SIS 2134). Chemical composition, tension test data and notch toughness are given in Table 1 - 3. The fracture toughness of the parent metal is $J_c$ = 175 N/mm at -20 °C and greater than 200 N/mm at room temperature.

TABLE 1 Chemical composition (weight percent)

| C | Si | Mn | P | S | N | Cr | Ni | Cu | V | Al | O(ppm) |
|---|---|---|---|---|---|---|---|---|---|---|---|
| .15 | .35 | 1.35 | .012 | .020 | .010 | .07 | .06 | .07 | .09 | .008 | 77 |

TABLE 2 Tension test data

| $R_e$ | $R_m$ | $A_5$ | Z |
|---|---|---|---|
| 380 N/mm$^2$ | 540 N/mm$^2$ | 30 % | 74 % |

TABLE 3 Notch toughness

| temp | -40 | -20 | 0 | +20 °C |
|---|---|---|---|---|
| U(Nm) | 85 | 155 | 161 | 163 |

From plates of the parent metal (thickness 25 mm) were machined coupons 500 x 1000 mm. Gas cutting was used for joint preparation. Pairs of the coupons were welded together such that welds with length 1000 mm perpendicular to the rolling direction of the parent plate were obtained. The welding method was submerged arc welding. Welding data (Table 4) and joint dimensions (Fig. 1) were chosen according to common practice. All welds were tested radiographically to 100 % and those with degree 3 or lower were rejected. Chemical composition of the weld metals are given in Table 5.

TABLE 4 Welding methods, welding positions and filler metals

| Weld | Method | Position | Type | Notation (DIN 1319 and 8557 ISO) |
|---|---|---|---|---|
| I | Submerged arc welding | Twoside, single electrode, multi-run | High basic welding flux | S 2 Mo, 12 ay 457 |
| II | Submerged arc welding | Oneside tandem welding, 2 runs | High basic welding flux | S 2 Mo, 12 b 457, ok Grain 21.81, ok Backing 21.82 |

TABLE 5 Chemical composition (weight percent), weld metals

| Weld metal | C | Si | Mn | P | S | Cr | Ni | Cu | Nb | Al | V | Mo | O(ppm) |
|---|---|---|---|---|---|---|---|---|---|---|---|---|---|
| I | 0.13 | 0.35 | 1.19 | 0.026 | 0.030 | 0.175 | 0.129 | 0.071 | 0.005 | 0.012 | 0.058 | 0.258 | 445 |
| II | 0.12 | 0.21 | 0.96 | 0.023 | 0.017 | 0.059 | 0.099 | 0.099 | 0.004 | 0.009 | 0.033 | 0.294 | 227 |

Throughout the fracture toughness testing the standard method (ASTM, 1973) has been adhered to when applicable. Three point bend specimens were machined from the welded coupon pairs and fatigued in room temperature. The notch and crack orientation in the weld metals is shown in Fig. 2. The fracture toughness was determined at the temperatures -40, -10 and +20 °C. Due to the amount of plastic deformation which preceeded fracture, the load-deflection relationships were in general nonlinear. The fracture toughness was accordingly evaluated with nonlinear theory and a critical value of the J-integral was determined by using a method suggested by Rice (1968). To determine one fracture toughness value was used a series of three specimens. The results are shown in Fig. 3.



## FRACTOGRAPHY AND METALLOGRAPHY

The fracture surfaces were studied with a low-magnifying lens and a scanning electron microscope. The domain immediately ahead of the fatigue crack tip, where initiation of fracture is most likely to take place, was prepared for a metallographic study. One of the halves of each broken specimen were cut perpendicular to the crack plane and parallel to the fatigue crack tip so that the profile of the crack surface is seen on these sections. The polished and etched surfaces were studied in a light microscope.

## RESULT

### Fractography

The macroscopic view of the fracture surfaces are shown in Fig. 3. The fracture surfaces comprise generally three distinct regions: a central, flat, with a needle-like lustrous structure, lateral shear lips with a lustreless structure, and a region immediately ahead of the fatigue crack tip also with a lustreless structure.

The main difference between the materials and at the different test temperatures is the relative extent of these regions. For weld metal I at +20 °C the central flat region is absent altogether.

The SEM study reveals that the fracture surface within the lustreless regions is covered with dimples. In regions with needle-like lustrous structure the fracture mechanism is of a mixed type: mainly quasi-cleavage with some few solitary dimple regions.

The most interesting feature is the fact that in both weld metals and at all temperatures there exists a narrow region immediately ahead of the fatigue crack tip which is covered with dimples. The extent of this region in the growth direction of the macroscopic fracture ($\Delta S$) is varying along the fatigue crack tip in both materials and is not always continuous in weld metal II. An estimate of the mean extent of $\Delta S$ is shown in Table 6.

TABLE 6 $\Delta S$ (mm)

| Temperature °C | Weld metal I | Weld metal II |
|---|---|---|
| +20 | overall | (0 - ) .125 |
| -10 | .700 | (0 - ) .040 |
| -40 | .030 | (0 - ) .010 |

It is difficult to estimate the surface fractions of the two fracture mechanisms. Nevertheless it is clear that the fraction of the mixed mechanism decreases with temperature and that the fraction of the mixed mode for a given temperature is greater in weld metal II than in I.

### Metallography

Sections of the fracture surface just ahead of the fatigue crack tip where initiation of fracture most likely takes place are shown in Figs. 4 - 11. The micro-structure of the two weld metals consists of mainly acicular ferrite and proeutectoide ferrite, and some retained austenite and martensite. The complexity of the structures renders any quantitative estimate almost impossible. The characteristical differences between the two weld metals are however: a) the grains are coarser in weld metal II, b) the fraction of proeutectoide ferrite is greater in weld metal II, c) the proeutectoide

ferrite appears in weld metal II mainly as elongated, broad bands which are often interconnected, whereas in weld metal I as short, narrow bands or islands which are isolated from each other.

The fracture in weld metal I is entirely ductile at +20 °C, Fig. 12. For lower temperatures some few solitary cleavage facettes appear in a mainly ductile fracture, Figs. 13-14. The fracture in weld metal II is a mixed fracture and the fraction of cleavage facettes is much greater than for weld metal I, Figs. 15-17.

The plastic deformation in the fracture surface and fraction ductile fracture is increasing with temperature. The cleavage facettes appear within the bands of proeutectoide ferrite whereas the fracture mechanism is ductile in the acicular ferrite.

The elongated, interconnected bands of proeutectoide ferrite in weld metal II are very attractive domains for propagation of local cleavage fractures.

## DISCUSSION

There are generally two distinct fracture mechanisms in the weld metals: one ductile and one brittle. The ductile mechanism is characterized by formation of holes around inclusions and their subsequent growth and coalescence and is asscciated with dimples on the fracture surface. For a given volume fraction of inclusions the fracture work decreases with yield stress and increases with hardening. The fracture work is also rather independent of the grain size of the material and the temperature (Tetelman and McEvily, 1967). The brittle mechanism is characterized by the formation and growth of microcracks within single grains and their subsequent coalescence. This mechanism is associated with the cleavage facettes on the fracture surface. Initiation and stable growth of a microcrack requires an effective barrier for the motion of dislocations and is governed by the local shear stress concentration. The unstable growth is on the other hand governed by the stress normal to the crack plane (Tetelman and McEvily, 1967). The growth of a microcrack can be discontinuous. If a growing microcrack encounters a strong enough barrier its growth is interrupted. Reinitiation follows only if the applied stress is increased enough. The discontinuous growth may be repeated until unstable growth of the gross fracture of the entire specimen follows.

The maximum distance between barriers capable of arresting a growing crack is then decisive for the overall unstable fracture. As grain boundaries are very effective barriers for the growth of a microcrack the condition for the final reinitiation must be strongly dependent of the grain size. In a polycrystal where some grains fail through cleavage and others through a ductile mechanism (at the same temperature) it is clear that the grain size of the former is decisive for the size of the microcracks which trigger the final fracture.

The initiation of the overall fracture is ductile and stable for both weld metals at all temperatures. In the domain just ahead of the fatigue crack tip where a triaxial stress state arises local cleavage microcracks are formed. The growth of the microcracks may be discontinuous and the macroscopic fracture follows when the condition for unstable growth of the largest microcracks is fulfilled locally. Assuming that the fracture toughness depends on the extent of stable crack growth the transition to unstable crack growth determines the fracture toughness of the material.

The fracture toughness of the weld metals is however not a function of $\Delta S$ only, where $\Delta S$ is the mean extent of the stable crack growth. It is important to point out that the region of stable crack growth is not continuous in weld metal II. This illustrates the strong detrimental effect of local microcracks upon the fracture toughness of the material.

The microstructural difference between the weld metals are mainly grain size and



content and distribution of proeutectoide ferrite. The crystal lattice of proeutectoide ferrite is homogeneous with closed-packed planes while the grains of acicular ferrite have a complex lath substructure. Thus a microcrack propagates much more easily through proeutectoide ferrite than through acicular ferrite.

Maximum length and width of imagined planes that can be thought of as inscribed in the domains of proeutectoide ferrite are much greater for weld metal II than for I. A microcrack can therefore extend over a much longer plane before a barrier is encountered in this material. The important geometrical parameter of the condition for unstable growth of a microcrack is the crack length. The critical stress for growth is proportional to $1/\sqrt{\text{crack length}}$. Reinitiation and transition of unstable growth thus occur at a much lower stress in weld metal II, a fact which explains the lower fracture toughness of this material. To account for the difference of fracture toughness at e.g. -10 °C, or the maximum differences between the materials, the "free extension path" of a microcrack must have a characteristical length in weld metal II which is 5 times that of weld metal I. A comparison with the fractographic and metallographic studies reveals that this condition is well fulfilled.

Owen and co-workers (1957) have found that in a Widmanstätten structure the ferrite may behave as though it had an unexpectedly large grain size and conclude that fracture paths may exist in such structures which are much longer than that corresponding to the average linear dimension. The interesting effect is a higher Charpy transition temperature for Widmanstätten structures at any given grain size.

Cane and Dolby (1974) have studied the HAZ fracture toughness of C-Mn-steel produced by submerged arc welding. They considered proeutectoide ferrite to be beneficial for the fracture toughness of their materials. Recent works by e.g. Otterberg (1979) and Stenbacka (1980) show on the other hand a detrimental effect of proeutectoide upon toughness in thermally simulated weld metals. Thus, at the present time it seems reasonable to conclude that proeutectoide per se is not necessarily detrimental for the fracture toughness of weld metals, but that other factors e.g., as found in this work, the relative content and distribution of the proeutectoide ferrite play the important role for the beneficial, if any, or detrimental effect upon the fracture toughness of weld metals.

## REFERENCES


ASTM (1973). Standard method of test for plane-strain fracture toughness of metallic materials. E399-72. In 1973 Annual Book of ASTM Standards. ASTM. Philadelphia.

Cane, M.W.F., and R.E. Dolby (1974). Metallurgical factors controlling the HAZ fracture toughness of submerged-arc welded C-Mn steels. Welding Res. Inst., 4, pp. 351-372.

Eriksson, K. (1979). $J_{Ic}$-fracture toughness testing of some weld metals in Sweden. IIW Annual Assembly 1979, Bratislava. pp. 150-159.

Otterberg, R., A. Sandberg, and R. Sandström (1977). Influence of Widmanstätten-ferrite on the mechanical properties of microalloyed steel. Report IM-1225. Swedish Institute for Metal Research, Stockholm.

Owen, W.S., D.H. Whitmore, M. Cohen, and B.L. Averbach (1957). The relation of Charpy impact properties to the microstructure of three ship steels. The Welding Journal Res. Suppl., 36, p. 503.

Rice, J.R. (1968). A path independent integral and the approximate analysis of strain concentrations by notches and cracks. J. Appl. Mech., 35, pp. 379-386.

Stenbacka, N.M.W. (1980). Mechanical properties of some structural steels before and after simulation of thermal cycles in welding. Ph.D. Thesis. Dept. of Welding Technology. The Royal Institute of Technology. Stockholm.

Tetelman, A.S., and A.J. McEvily (1967). Fracture of structural materials. John Wiley & Sons Inc. New York.

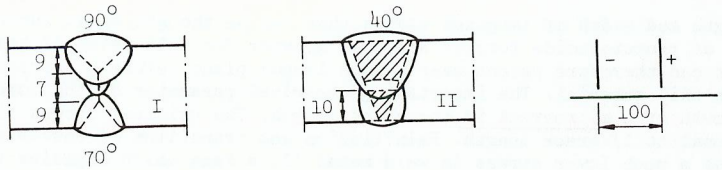


Fig. 1. Joint dimensions for Weld metals I and II.

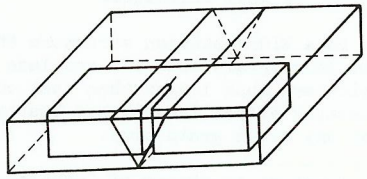

Fig. 2. Three point bend specimen orientation in the weld metal.

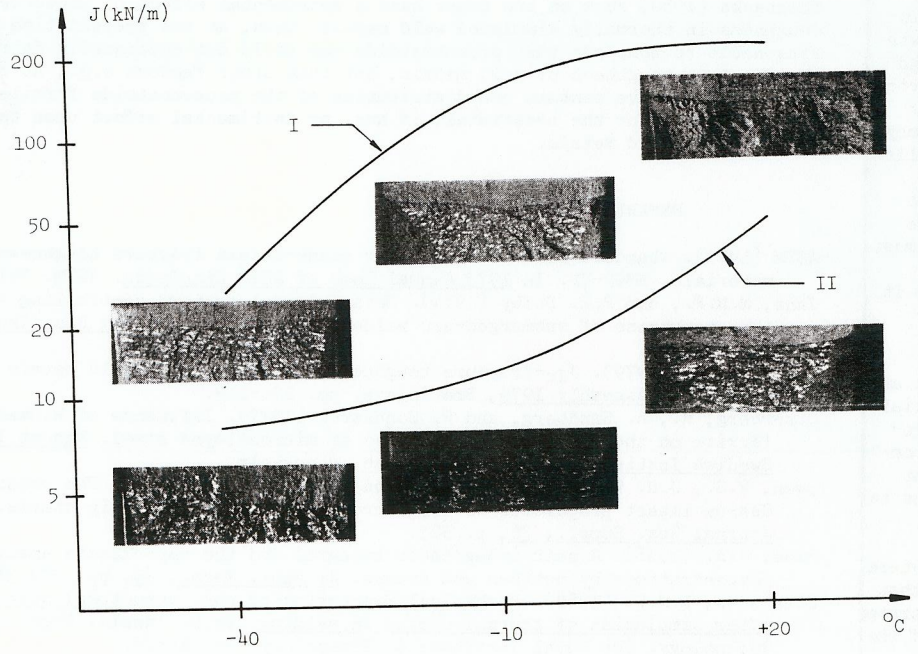


Fig. 3. Fracture toughness of Weld metal I and II.



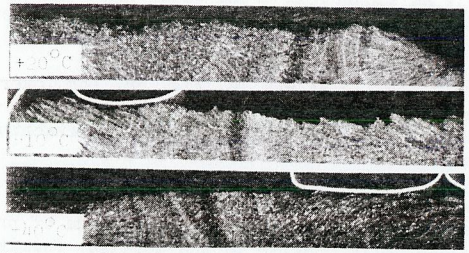

Fig. 4. Fracture surface in Weld Metal I. 4x

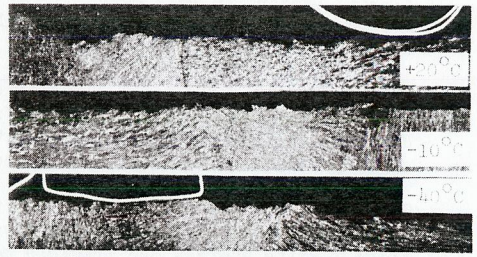

Fig. 5. Fracture surface in Weld Metal II. 4x

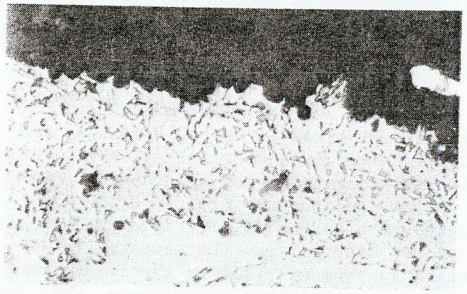

Fig. 6. Weld Metal I +20°C. 700x

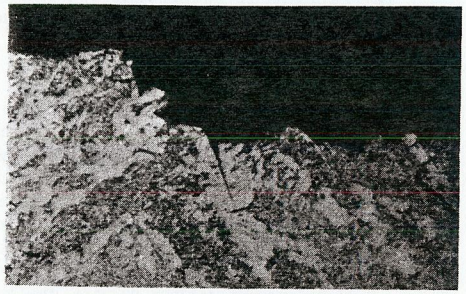

Fig. 9. Weld Metal II +20°C. 140x

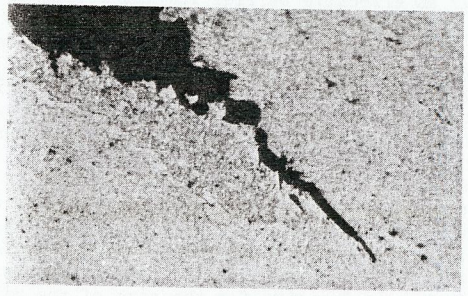

Fig. 7. Weld Metal I -10°C. 280x

Fig. 10. Weld Metal II -10°C. 700x

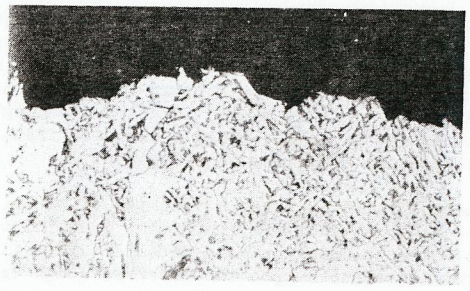

Fig. 8. Weld Metal I -40°C. 700x

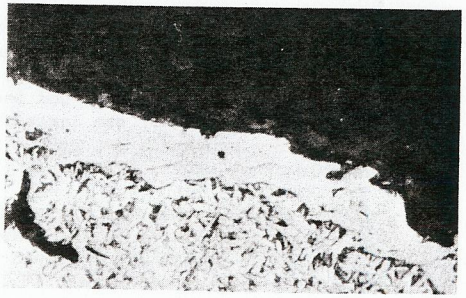

Fig. 11. Weld Metal II -40°C. 700x

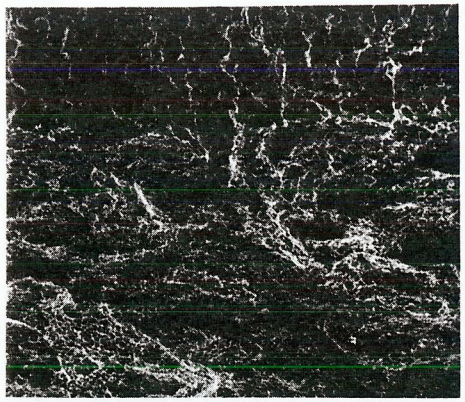

Fig. 12. Weld Metal I +20°C. 200x

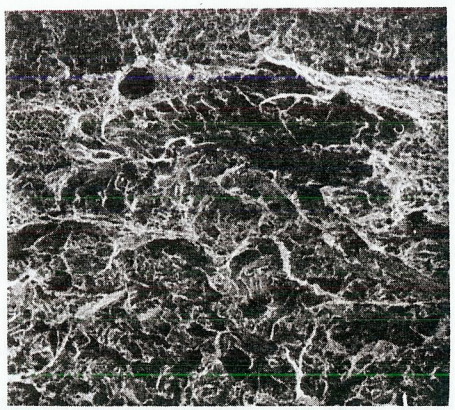

Fig. 15. Weld Metal II +20°C. 200x

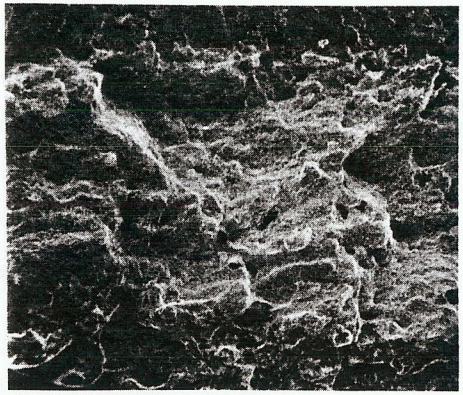

Fig. 13. Weld Metal I -10°C. 70x

Fig. 16. Weld Metal II -10°C. 300x

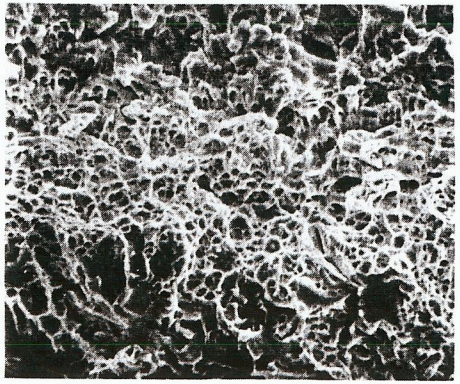

Fig. 14. Weld Metal I -40°C. 1000x

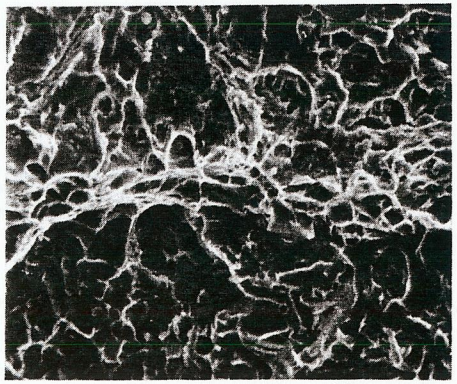

Fig. 17. Weld Metal II -40°C. 1000x